doi:10.1093/brain/aww023 BRAIN 2016: 139; 1539–1550 | 1539

BRAIN
A JOURNAL OF NEUROLOGY

Regional profiles of the candidate tau PET ligand ^{18}F-AV-1451 recapitulate key features of Braak histopathological stages

Adam J. Schwarz,[1] Peng Yu,[1] Bradley B. Miller,[1] Sergey Shcherbinin,[1] James Dickson,[2] Michael Navitsky,[2] Abhinay D. Joshi,[2] Michael D. Devous Sr[2] and Mark S. Mintun[2]

See Thal and Vandenberghe (doi:10.1093/brain/aww057) for a scientific commentary on this article.

Post-mortem Braak staging of neurofibrillary tau tangle topographical distribution is one of the core neuropathological criteria for the diagnosis of Alzheimer's disease. The recent development of positron emission tomography tracers targeting neurofibrillary tangles has enabled the distribution of tau pathology to be imaged in living subjects. Methods for extraction of classic Braak staging from *in vivo* imaging of neurofibrillary tau tangles have not yet been explored. Standardized uptake value ratio images were calculated from 80–100 minute ^{18}F-AV-1451 (also known as T807) positron emission tomography scans obtained from $n = 14$ young reference subjects (age 21–39 years, Mini-Mental State Examination 29–30) and $n = 173$ older test subjects (age 50–95 years) comprising amyloid negative cognitively normal ($n = 42$), clinically-diagnosed mild cognitive impairment (amyloid positive, $n = 47$, and amyloid negative, $n = 40$) and Alzheimer's disease (amyloid positive, $n = 28$, and amyloid negative, $n = 16$). We defined seven regions of interest in anterior temporal lobe and occipital lobe sections corresponding closely to those used as decision points in Braak staging. An algorithm based on the Braak histological staging procedure was applied to estimate Braak stages directly from the region of interest profiles in each subject. Quantitative region-based analysis of ^{18}F-AV-1451 images yielded region of interest and voxel level profiles that mirrored key features of neuropathological tau progression including profiles consistent with Braak stages 0 through VI. A simple set of decision rules enabled plausible Braak stages corresponding to stereotypical progression patterns to be objectively estimated in 149 (86%) of test subjects. An additional 12 (7%) subjects presented with predefined variant profiles (relative sparing of the hippocampus and/or occipital lobe). The estimated Braak stage was significantly associated with amyloid status, diagnostic category and measures of global cognition. *In vivo* ^{18}F-AV-1451 positron emission tomography images across the Alzheimer's disease spectrum could be classified into patterns similar to those prescribed by Braak neuropathological staging of tau pathology.

1 Tailored Therapeutics, Eli Lilly and Company, Indianapolis, IN 46285, USA
2 Avid Radiopharmaceuticals, Philadelphia, PA 19104, USA

Correspondence to: Adam J Schwarz,
Eli Lilly and Company,
DC 0725, Lilly Corporate Center,
835 S Delaware St,
Indianapolis, IN 46285, USA
E-mail: a.schwarz@lilly.com

Keywords: tau; 18F-AV-1451; Braak staging; imaging; positron emission tomography (PET)

Abbreviations: ADAS-Cog = Alzheimer's Disease Assessment Scale-Cognitive subscale; FBP = florbetapir; MCI = mild cognitive impairment; MMSE = Mini-Mental State Examination; SUVR = standardized uptake value ratio

Received September 30, 2015. Revised January 06, 2016. Accepted January 11, 2016. Advance Access publication March 2, 2016

Introduction

Post-mortem staging of neurofibrillary tau tangles using the Braak staging scheme is one of the core neuropathological criteria for the diagnosis of Alzheimer's disease encapsulated in recent NIA-AA guidelines (Hyman *et al.*, 2012; Montine *et al.*, 2012). Notably, cross-sectional autopsy studies of tau pathology in typical Alzheimer's disease suggest a well-defined neuroanatomical signature, hypothesized to begin focally in the transentorhinal cortex before first spreading medially into the hippocampus, then laterally around the temporal lobe, and thereafter into association regions of the frontal, parietal and occipital cortices (Braak and Braak, 1991; Braak *et al.*, 2006). The Braak staging scheme thus provides a principled means of staging the progression of tau pathology—one of the core hallmarks of Alzheimer's disease.

Until very recently, the only *in vivo* biomarker assay of tau pathology has been the measurement of tau and phospho-tau proteins from CSF samples obtained via lumbar puncture (Toledo *et al.*, 2013). This has been widely used in clinical Alzheimer's disease research and has identified increases above normal levels in the mild cognitive impairment (MCI) and dementia stages of Alzheimer's disease (Buchhave *et al.*, 2012). The recent development of candidate PET imaging tracers targeting aggregated tau (Chien *et al.*, 2013; Maruyama *et al.*, 2013; Okamura *et al.*, 2014; Villemagne and Okamura, 2014) now enables not only the brain burden but also the anatomical distribution of tau pathology to be mapped directly in living subjects. One such PET tracer, ^{18}F-AV-1451 (also known as ^{18}F-T807), has been shown to bind selectively to paired-helical filament (PHF) tau versus amyloid-β, α-synuclein and TDP-43 deposits in human brain tissues (Xia *et al.*, 2013; Marquie *et al.*, 2015), and to exhibit favourable kinetics, low non-specific binding and differential uptake in Alzheimer's disease versus healthy control subjects (Chien *et al.*, 2013). Initial *in vivo* observations showed tracer binding patterns that were qualitatively different than those observed with amyloid tracers and overlapping with areas of plausible PHF-tau deposition (Chien *et al.*, 2013). This imaging tool thus opens the possibility of staging the spread of tau pathology *in vivo*, longitudinally and across the disease spectrum prior to end-stage disease. This could have positive implications for clinical research in Alzheimer's disease and other neurodegenerative disorders, enabling a more refined selection of subjects for inclusion and/or stratification.

Our primary aim in the present study was to systematically assess, in a large subject sample, the consistency between the *in vivo* distribution of ^{18}F-AV-1451 binding and the well-established patterns of tau pathology encapsulated in the Braak staging scheme, and to test a simple mathematical algorithm for the automated assignment of an *in vivo* estimated Braak stage. Specifically, we defined a targeted set of regions of interest based closely on the Braak histopathology protocol, and sought to determine the extent to which regional profiles across these regions of interest and in the overall radiotracer binding maps reflected expected patterns of typical Alzheimer's disease tau pathological progression. Moreover, as both tau and amyloid-β are defining brain pathologies in Alzheimer's disease (Hyman *et al.*, 2012; Montine *et al.*, 2012), and understanding the relationship between them is central to current models of the disease (Jack *et al.*, 2013; Stancu *et al.*, 2014), a secondary aim was to determine the relationship between the severity of tau pathology, assessed by ^{18}F-AV-1451 imaging, and amyloid status, assessed by ^{18}F-florbetapir (FBP) imaging.

Materials and methods

Subjects and data acquisition

All subjects gave informed consent to participation in one of two clinical studies of ^{18}F-AV-1451: an early exploratory trial and a larger phase 2 study (NCT 02016560). Fourteen young cognitively normal subjects, drawn from both studies, were used as a reference dataset. One hundred and seventy-three older subjects from the second study only, comprising older cognitively normal, MCI and Alzheimer's disease dementia diagnostic categories, were used to test the Braak staging procedure. Subjects in the older cognitively normal group were $\geqslant$50 years old and had a Mini-Mental State Examination (MMSE) score $\geqslant$29. Subjects in the MCI group were $\geqslant$50 years old, MMSE $\geqslant$24 and diagnosed clinically with MCI consistent with the NIA-AA guidelines (Albert *et al.*, 2011). Subjects in the Alzheimer's disease group were $\geqslant$50 years old, MMSE $\geqslant$10 and diagnosed clinically with possible or probable Alzheimer's disease consistent with the NIA-AA guidelines (McKhann *et al.*, 2011). More detailed inclusion criteria are provided in the Supplementary material. Cases with clinical presentations suggestive of non-Alzheimer's disease tauopathies were excluded from this trial. However, subjects determined as amyloid negative based on an ^{18}F-FBP PET scan were retained, in order to assess the relationship between amyloid status and estimated Braak stage based on the ^{18}F-AV-1451 scans.

The ^{18}F-AV-1451 PET data acquisition included four 5-min whole-brain frames spanning 80–100 min post-injection of ~10 mCi ^{18}F-AV-1451. All subjects also underwent an ^{18}F-FBP amyloid PET scan (50–60 min post-injection of 10mCi ^{18}F-FBP) on a separate day to determine brain amyloid load. Three dimensional T_1-weighted structural MRI scans were also acquired on all subjects for use in the postprocessing of the ^{18}F-AV-1451 PET data.

Image processing

For each subject, the four 5-min ^{18}F-AV-1451 PET frames first were motion-corrected (FSL/McFLIRT) and averaged to yield a single 3D image. Both PET and MRI images were then skull stripped to retain only signal from brain parenchyma (FSL/BET) and the PET image was then affine co-registered to the MRI brain. Next, the MRI image was spatially normalized to

the Montreal Neurological Institute (MNI) T_1 MRI brain template using the segment/normalize function in SPM8 with a heavily-regularized non-linear transformation. This generates a spatial transformation from individual subject to standard space as well as individually segmented maps of grey matter, white matter and CSF. The same spatial transformation was then applied to the accompanying ^{18}F-AV-1451 PET image, and standardized uptake value ratio (SUVR) images were calculated using a cerebellar crus reference region, sampling cerebellar grey matter.

FBP-PET images were spatially normalized to MNI space (SPM) and converted to SUVR values using the whole cerebellum as a reference region (Joshi *et al.*, 2015). A composite SUVR score was then computed as the average of the mean SUVR in each of six predefined atlas-based regions of interest, and a cut-off of 1.1 was used to determine amyloid positivity.

Regions of interest corresponding to brain sections used in Braak staging

The original Braak staging protocol described the brain regions characteristic of the spread of tau pathology from the medial temporal lobe to the broader neocortex, and an associated staging scheme (Braak and Braak, 1991). More recently, a revised methodological protocol precisely specified histological sections in the anterior temporal and occipital lobes for staining by phospho-tau immunohistochemistry along with more explicit decision rules with the aim of more uniform application (Braak *et al.*, 2006). We defined regions of interest based on standard brain imaging atlases to sample the 3D PET images in locations corresponding closely to the slices specified in this more recent, operationalized Braak staging protocol (Braak *et al.*, 2006). All regions of interest were defined in MNI space, based on a 2 mm isotropic voxel matrix.

In the anterior temporal lobe, the Braak staging protocol specifies two coplanar sections to stage neurofibrillary pathology in the earlier stages of Alzheimer's disease. One section is taken medially to assess tau pathology in the entorhinal and hippocampal regions found in the earliest stages, while the other is taken laterally to assess involvement of the middle and superior temporal gyri as the pathology spreads to neocortical structures in later stages. However, the division of this cut into two sections is only for compatibility with standard histological tissue cassettes—the use of a single, larger section is permitted by the staging protocol (Braak *et al.*, 2006). The cutting line is at the mid-uncal level, coinciding with the anterior parahippocampal gyrus, the anterior most aspect of the hippocampal formation and intersecting the rhinal sulcus on the inferior medial aspect of the temporal lobe. Transversely, the section intersects anterior portions of the occipito-temporal (fusiform) gyrus, and the inferior, middle and superior temporal gyri.

Our anterior temporal lobe regions of interest were defined by the intersection of atlas structures and a coronal section extending from MNI coordinates $y = 57$–61 to define a 1-cm thick slab, encompassing the uncus and the anterior most aspect of the hippocampus. The Harvard-Oxford probabilistic atlas (provided as part of the FSL distribution, http://www.fmrib.ox.ac.uk/fsl) was used to define regions of interest from the hippocampus, fusiform gyrus, middle temporal gyrus and superior temporal gyrus (Fig. 1A). Anterior and posterior divisions of the latter four atlas structures were fused beforehand because the anterior/posterior boundaries in the atlas lay within our target region coverage.

In the entorhinal cortex, our region of interest was based on the histologically defined delineation of this structure mapped into MNI space and provided as part of the Juelich histological atlas (Amunts *et al.*, 2005) (distributed with FSL). As the earliest manifestation of neurofibrillary pathology is focally restricted to the transentorhinal region (Braak and Braak, 1991; Braak *et al.*, 2006), located in the mesial aspect of the rhinal sulcus, we truncated the atlas structure to retain only voxels with MNI coordinates $z < 21$. This restricted the region of interest to the inferior portion of the entorhinal cortex and aligns more closely to the transentorhinal region whilst maintaining a reasonable region of interest size for quantification (Fig. 1). Because the resulting region of interest extended slightly into the Harvard-Oxford fusiform gyrus region of interest, we removed the overlapping voxels from the fusiform gyrus region of interest.

In the occipital lobe, the Braak staging section is cut halfway between the occipital pole and the intersection of the calcarine fissure with the parieto-occipital sulcus, inferior to and perpendicular to the calcarine fissure (Braak *et al.*, 2006). This block is used to assess pathological involvement of the striate area (primary visual cortex; BA17) versus the adjacent peri-striate and para-striate regions in the later (cortical) neurofibrillary stages of Alzheimer's disease. For our occipital lobe regions of interest, we used the histologically defined regions corresponding to primary (V1) and higher (V2–V4) visual cortices in the Juelich atlas. Since the later Braak stages are distinguished by the relative presence of pathology in striate (V1) versus extrastriate (V2–V4) areas, we combined the regions V2–V4 into a single extrastriate region. To define a section corresponding to the location and angle specified by Braak *et al.* (see above) we rotated the MNI template image by 25°, enabling a section in the x–z plane ($17 < x < 74$, $35 < y < 40$ and $12 < z < 27$) to be defined perpendicular to the calcarine fissure halfway between the occipital pole and the junction with the parieto-temporal sulcus. This slab mask was then transformed back into MNI space using the inverse transformation and voxels within the striate and extrastriate structure masks intersecting this slab were retained (Fig. 1B).

The signal in each region of interest was quantified as the mean value of voxels lying both within the region of interest mask and the individual subject grey matter mask (thresholded at 25%), in order to mitigate against signal dilution in the presence of substantial brain atrophy.

Additional regions of interest

We used 3D masks from the Harvard-Oxford cortical atlas to sample ^{18}F-AV-1451 uptake in additional regions outside the standard Braak areas, namely the angular gyrus, precuneus, mid-frontal gyrus, precentral gyrus and the amygdala.

Algorithm for estimating Braak stages from region of interest SUVR profiles

A set of 14 young cognitively normal subjects were determined to be 'tau negative' based on visual inspection and a mean bilateral SUVR < 1.2 in the transentorhinal cortex region of

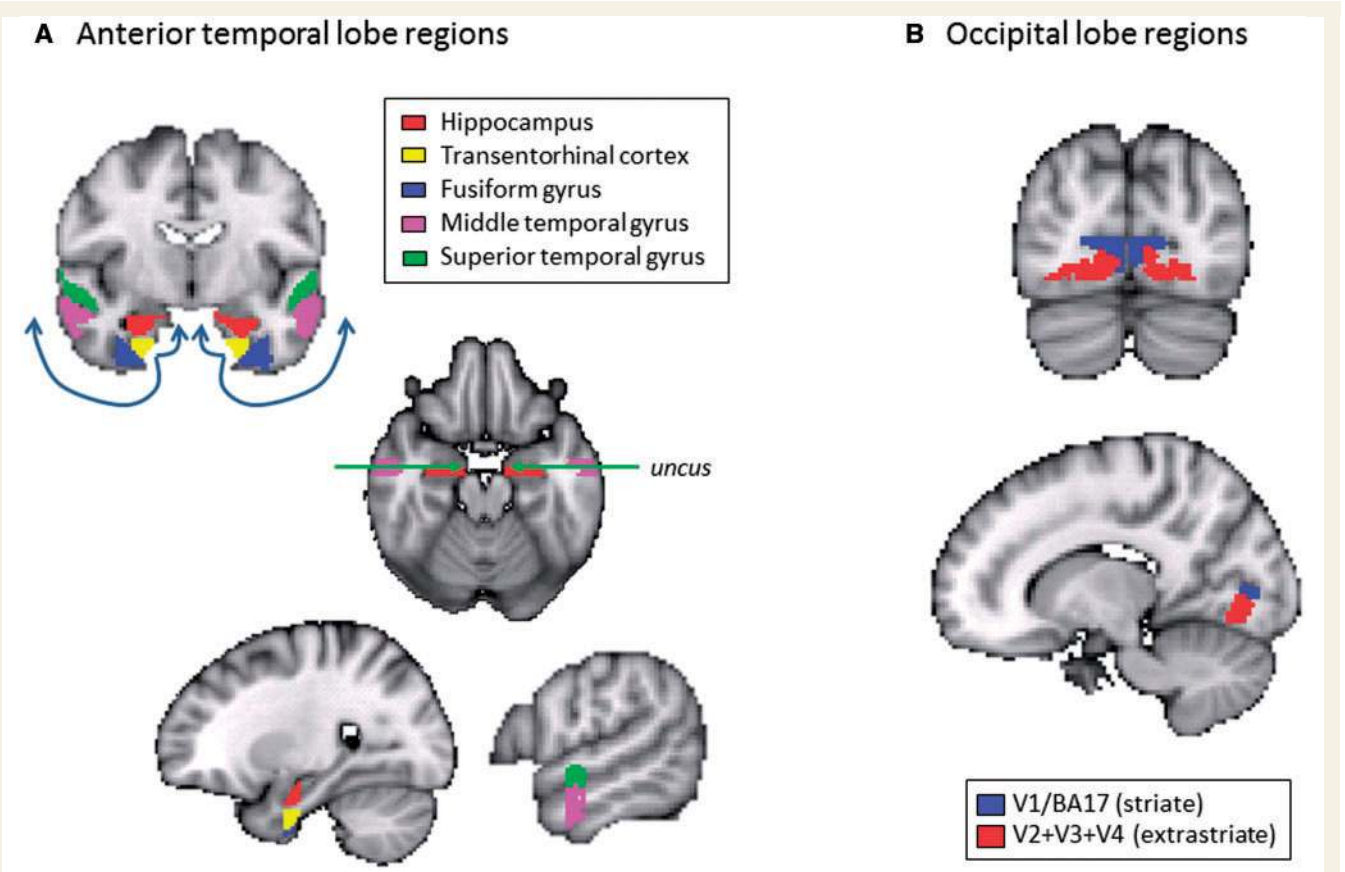

Figure 1 Regions of interest chosen to match histological slices and key brain structures prescribed by the Braak staging protocol (Braak et al., 2006) located in (A) the anterior temporal lobe and (B) the occipital cortex. Arrows in (**A**) designate the stereotypical progression of tau pathology, starting from the transentorhinal cortex.

interest. This reference set was used to define region of interest-wise positivity thresholds at a SUVR value of 2.5 standard deviations (SD) above the mean across the 28 hemispheres, so that $<1\%$ of supra-threshold values would be false positives. These cut-off values ranged from 1.22 (superior temporal gyrus) to 1.36 (fusiform cortex). This threshold profile was then applied to region of interest mean SUVR values from the $n = 173$ subjects in the test cohort to generate binary region of interest profiles for each hemisphere from each subject.

A set of rules based on the Braak neuropathological staging scheme (Braak and Braak, 1991; Braak *et al.*, 2006) was used to map the binary region of interest profiles to estimated Braak stage 0–VI. The algorithm is shown schematically in Supplementary Fig. 1, and proceeds as follows for each test subject. First, the binarized region of interest profile from each hemisphere is tested for a match to one of the seven stereotypical patterns of tau spreading (Table 1) and assigned a numeric value 0 through 6 corresponding to the associated Braak stage; profiles not matching any expected pattern are assigned a value of −1. Each hemisphere was staged independently, and the subject-level estimated Braak stage is calculated as the maximum of the two hemispheres. If neither hemisphere matches a stereotypical pattern, the profiles are matched in a similar fashion to specific variant profiles (Table 2), capturing a typical pattern in the anterior temporal neocortex but sparing of the hippocampus or visual cortex. Subjects for whom neither hemisphere satisfies either a typical or an atypical variant profile remained as unassigned and were examined individually, with special attention to evaluating whether supra-threshold signal in the Braak regions indicated involvement despite absence of regions expected earlier in the pathological progression.

Statistical analysis

All analyses were conducted by JMP v11 (SAS, Cary, NC, USA). The relationship between estimated Braak stage and diagnostic category, MMSE and Alzheimer's Disease Assessment Scale-Cognitive subscale (ADAS-Cog_{13}) was assessed using ordinal logistic regression with age, sex and amyloid status as covariates. The relationship between estimated Braak stage and FBP-PET composite SUVR value was assessed using ordinal logistic regression with age and sex as covariates. Ordinal logistic regression was used because stages were ordered. Entropy R^2 was used to evaluate the goodness-of-fit and the *P*-values of the regression coefficients were reported for diagnostic category, MMSE, ADAS-Cog_{13} and FBP-PET to examine their contributions. Additionally, the relationships between regional ^{18}F-AV-1451 SUVR and each of ADAS-Cog_{13} and MMSE were assessed using linear regression with age, sex, and amyloid status as covariates. R^2 was reported for regional SUVR analysis as well for comparison with estimated Braak stage. An alpha-level of 0.05 was used as a threshold for statistical significance.

Table 1 Decision rules for stereotypical Braak stage estimation

Estimated Braak stage	Region of interest						
	HIP	TEC	FUS	MTG	STG	EVC	PVC
0	–	–	–	–	–	–	–
I	–	+	–	–	–	–	–
II	+	+	–	–	–	–	–
III	+	+	+	–	–	–	–
IV	+	+	+	+	–	+	–
V	+	+	+	+	+	+	–
VI	+	+	+	+	+	+	+

A plus (+) sign indicates that a region is positive (SUVR above region of interest-specific threshold) whereas a minus (–) sign indicates that a region is negative (SUVR below threshold). EVC = extrastriate visual cortex; FUS = fusiform gyrus; HIP = hippocampus; MTG = middle temporal gyrus; PVC = primary (striate) visual cortex; TEC = transentorhinal cortex; STG = superior temporal gyrus.

Table 2 Decision rules for assignment of specific variant profiles

Stage variant	Region of interest							Notes
	HIP	TEC	FUS	MTG	STG	EVC	PVC	
III.1	–	+	+	–	–	–	–	Hippocampal sparing
IV.1	–	+	+	+	–	+	–	Hippocampal sparing
IV.2	+	+	+	+	–	–	–	Visual cortex sparing
IV.3	–	+	+	+	–	–	–	Sparing of both hippocampus and visual cortex
V.1	–	+	+	+	+	+	–	Hippocampal sparing
V.2	+	+	+	+	+	–	–	Visual cortex sparing
V.3	–	+	+	+	+	–	–	Sparing of both hippocampus and visual cortex
VI.1	–	+	+	+	+	+	+	Hippocampal sparing

A plus (+) sign indicates that a region is positive (SUVR above region of interest-specific threshold) whereas a minus (–) sign indicates that a region is negative (SUVR below threshold). EVC = extrastriate visual cortex; FUS = fusiform gyrus; HIP = hippocampus; MTG = middle temporal gyrus; PVC = primary (striate) visual cortex; TEC = transentorhinal cortex; STG = superior temporal gyrus.

Results

Subject sample

Subject demographics in the test cohort are summarized in Table 3. Overall, 75/173 subjects (75/131 MCI or Alzheimer's disease) were amyloid positive. Amyloid positive MCI (MCI+) subjects did not differ significantly from amyloid negative MCI (MCI–) subjects in age or MMSE, but MCI+ subjects performed slightly worse than MCI– on ADAS-Cog ($P = 0.03$). Amyloid positive Alzheimer's disease dementia (AD+) subjects did not differ significantly from amyloid negative Alzheimer's disease dementia (AD–) subjects in age, MMSE or ADAS-Cog.

^{18}F-AV-1451 profiles recapitulate key features of Braak neuropathological progression

The *in vivo* ^{18}F-AV-1451 images in the present sample exhibited distributions of tau pathology consistent with those expected from post-mortem studies. Many subjects exhibited uniformly low cortical tracer signal of a similar magnitude to the reference region, some showed focal increased tracer retention in the medial temporal lobes consistent with Braak stages I–III, whereas others exhibited more widespread distributions of tracer binding that included lateral temporal, frontal and parietal association cortices, including the precuneus.

Across all five diagnostic categories, including both amyloid positive and amyloid negative subjects, the algorithm classified 149/173 (86%) of the subjects into one of the seven stereotypical Braak neuroanatomical profiles. Of these, 88 (51%) were assigned an estimated Braak stage of 0, whereas 61 (35%) exhibited a profile consistent with Braak stages 1 to 6 (Table 4).

A further 12 subjects (7%) had region of interest profiles that fit one of the predefined variants, with suprathreshold signals in the inferior and lateral temporal lobes but subthreshold signal (sparing) of the hippocampus and/or visual cortex (Table 4). Two of these subjects had profiles consistent with an atypical Braak stage IV profile, and 10 with atypical Braak stage V profiles. The majority of the variant profiles occurred in amyloid positive MCI or Alzheimer's disease subjects and corresponded to the visual cortex sparing variant of Braak stage V. These subjects had stereotypical involvement of the anterior temporal lobes, including the superior temporal gyrus, but anomalously low (subthreshold) signal in the extrastriate visual cortex.

Table 3 Demographics of subject sample

Category and amyloid status	*n* (% female)	Age mean (SD) [min–max]	MMSE mean (SD) [min–max]	ADAS-Cog mean (SD) [min–max]
OCN–	42 (45%)	67.3 (9.4) [52 – 84]	29.5 (0.5) [29 – 30]	6.4 (3.7) [1 – 17]
MCI–	40 (50%)	69.2 (8.7) [50 – 84]	28.2 (1.8) [24 – 30]	8.8 (4.2) [1 – 24]
MCI+	47 (45%)	72.6 (8.5) [50 – 92]	27.6 (1.8) [24 – 30]	11.2 (5.8) [0 – 34]
AD –	16 (50%)	72.4 (6.8) [62 – 87]	22.6 (2.8) [17 – 27]	17.8 (7.5) [8 – 38]
AD+	28 (64%)	74.3 (10.1) [54 – 95]	21.5 (4.5) [12 – 30]	22.4 (8.8) [8 – 47]

OCN = older cognitively normal.

Table 4 Breakdown of estimated Braak stages by diagnostic category

Estimated Braak stage		Number of subjects					
Stereotypical	**Variant**	**Total**	**OCN–**	**MCI–**	**MCI+**	**AD –**	**AD+**
Unclassified		12	3	4	4	0	1
0		88	36	31	12	8	1
I		7	1	1	2	3	0
II		9	0	1	5	2	1
III		8	0	1	4	1	2
	IV.1	*0*	*0*	*0*	*0*	*0*	*0*
IV		1	0	0	0	0	1
	IV.1	*0*	*0*	*0*	*0*	*0*	*0*
	IV.2	*1*	*0*	*0*	*0*	*0*	*1*
	IV.3	*1*	*0*	*0*	*1*	*0*	*0*
V		12	1	1	4	2	4
	V.1	*1*	*0*	*0*	*1*	*0*	*0*
	V.2	*7*	*0*	*0*	*3*	*0*	*4*
	V.3	*2*	*0*	*0*	*1*	*0*	*1*
VI		24	1	1	10	0	12
	VI.1	*0*	*0*	*0*	*0*	*0*	*0*

AD– = Alzheimer's disease, amyloid negative; AD + = Alzheimer's disease, amyloid positive; MCI– = mild cognitive impairment, amyloid negative; MCI+ = mild cognitive impairment, amyloid positive; OCN– = older cognitively normal, amyloid negative.

Stage-average SUVR maps and region of interest profiles showed patterns consistent with a progressive involvement of brain regions from the medial temporal lobe, spreading to the lateral temporal lobes and posteriorly to the visual cortex (Fig. 2). Note that only three subjects (one typical, two variant profiles) were assigned an estimated Braak stage of IV, of which one subject had a typical stage IV profile in the right hemisphere but a cyst in the left inferior temporal lobe, distorting the average stage IV image (Fig. 2E).

The remaining 12 subjects (7%) did not fit any of the stereotypical or variant profiles in either brain hemisphere (Supplementary material). Eight of 12 had MCI (four amyloid positive), 3/12 were older cognitively normal and 1/12 was in the Alzheimer's disease group (amyloid positive). Several of these subjects had relative sparing of parts of the medial temporal lobe structures despite suprathreshold signal in lateral temporal and/or occipital cortex. One Alzheimer's disease subject showed relatively strong binding throughout the staging regions but subthreshold signal in the transentorhinal cortex bilaterally, and two subjects were positive only in the hippocampus bilaterally.

Dependence of estimated Braak stages on diagnostic category and amyloid status

More advanced estimated Braak stages were strongly associated with the presence of brain amyloid (Fig. 3 and Table 4). Of those subjects with either typical or atypical

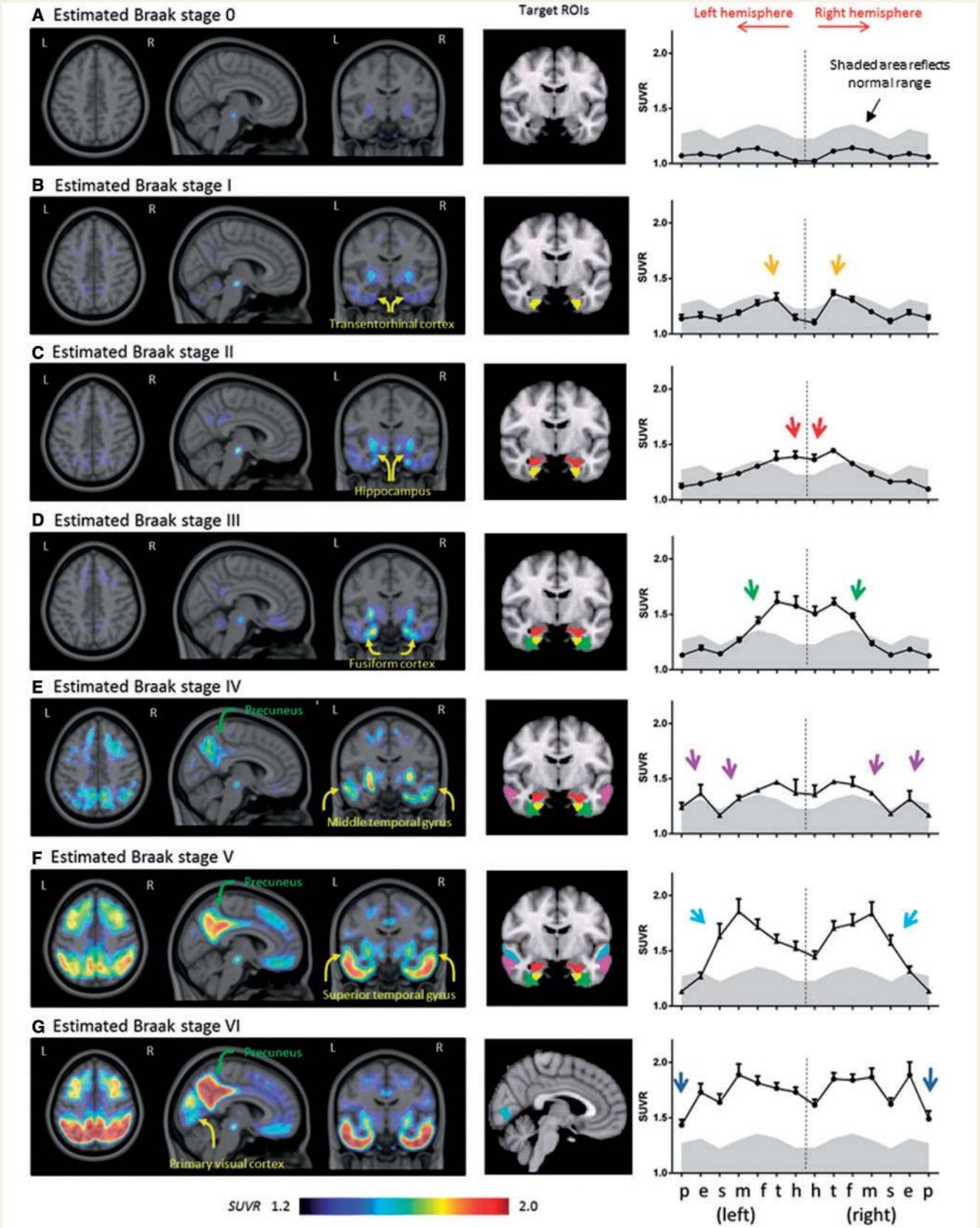

Figure 2 Average SUVR images and region of interest profiles by estimated Braak stage (stereotypical and variant patterns combined, representing 93% of the subjects in total). The region of interest profiles are presented in the form of 'butterfly plots', with the regions of interest from each hemisphere mirrored and ordered mediolaterally to reflect both the anatomical distribution and order of involvement with disease severity. The hippocampi are at the centre of the graphs and the occipital regions of interest at the lateral edges.

(continued)

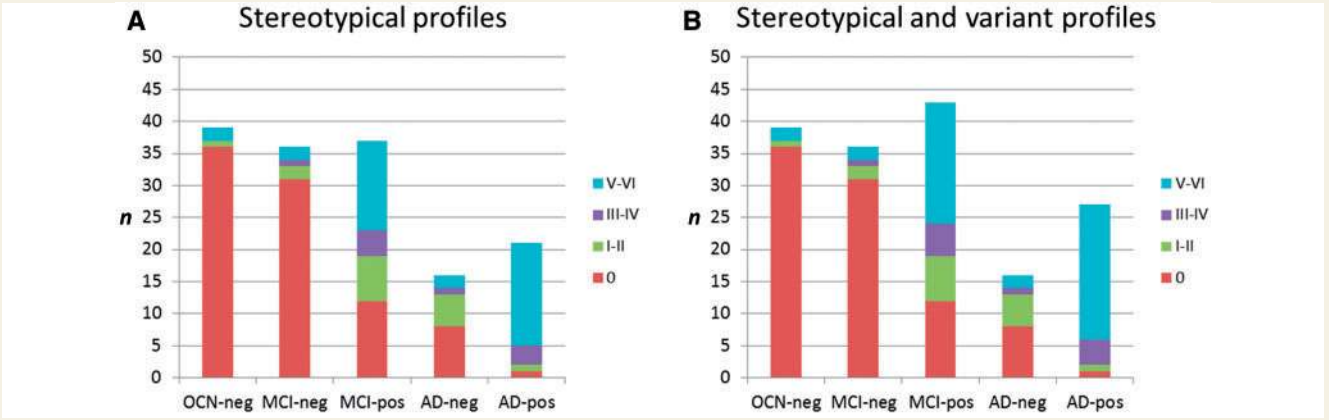

Figure 3 Distribution of estimated Braak stage by diagnostic category and amyloid status. OCN = older cognitively normal.

profiles, 92% of the amyloid negative older cognitively normal group was classified as having an estimated Braak stage of 0. The remaining three subjects (8%) had an estimated Braak stage >0, but were not outliers in terms of age. In both the MCI and Alzheimer's disease cohorts, the amyloid positive subjects had substantially greater estimated Braak stages overall than their amyloid negative counterparts. Eighty-six per cent of MCI− subjects but only 28% of MCI+ subjects, and 50% of AD− but only 4% of AD+ subjects were assigned an estimated Braak stage of 0. In the amyloid positive groups, the non-zero estimated Braak stages were skewed toward the more advanced isocortical stages; 19/31 (61%) of subjects with non-zero Braak stages in the MCI+ group, and 21/26 (81%) in the AD+ group, were assigned estimated Braak stages V or VI.

The estimated Braak stage was significantly and positively associated with both amyloid status ($P < 0.0001$) and diagnostic category ($P = 0.0002$), controlling for age and gender ($R^2 = 0.22$). The estimated Braak stage was significantly and positively associated with measures of global cognitive status (MMSE, $P = 0.0005$, $R^2 = 0.21$, and ADAS-Cog, $P = 0.0007$, $R^2 = 0.22$), controlling for age, gender and amyloid status. The estimated Braak stage was also positively associated with FBP-PET SUVR ($P < 0.0001$, $R^2 = 0.23$), controlling for age and gender.

Anatomical extent, intensity and intersubject variability

The estimated Braak stage algorithm, based on binarized region of interest profiles, is by construction a measure of anatomical extent and insensitive to the amplitude of suprathreshold tracer signal. We noted a high degree of variability in suprathreshold SUVR across subjects assigned the same estimated Braak stage (Fig. 4). This was particularly notable for neocortical regions in the isocortical stages V–VI. Regions involved earlier, such as the hippocampus, transentorhinal cortex and amygdala, also exhibited increased suprathreshold signal variability at earlier estimated Braak stages. Brain regions independent of the staging algorithm evidenced a similar range of trajectories—the amygdala signal was increased in stages I–II but only moderately more in stages III–VI, similar to the hippocampus, whereas neocortical regions in the frontal and parietal lobes evidenced the most marked increases in the isocortical stages only. Regions in the sensorimotor cortex increased only in the later stages but less dramatically than those in the association cortices (Fig. 4B and Supplementary Fig. 2).

Regional SUVR signal amplitudes correlated positively with measures of global cognition and explained more of the variance in the cognitive scales than the estimated Braak stage itself. SUVR in the anterior temporal lobe staging regions of interest was significantly associated with both MMSE and ADAS-Cog ($R^2 = 0.34$–0.44). Similarly, SUVR in association cortices (angular gyrus, precuneus and mid-frontal gyrus) was significantly associated with both MMSE and ADAS-Cog ($R^2 = 0.35$–0.43).

Discussion

In vivo tau PET images obtained using ^{18}F-AV-1451 exhibit topographical patterns of increased tracer binding

Figure 2 Continued

The vertical dashed line represents the midline and the shaded area the normal range and region of interest-wise threshold for positivity. Images are shown in neurological orientation (left = left), for consistency with the graphs. Note that one of the subjects with an estimated Braak stage of IV had a cyst in the left inferior temporal lobe, leading to signal dropout in that region of the average image (**E**); this subject's left hemisphere profile was removed from the calculation of the average region of interest plot. h = hippocampus; t = transentorhinal cortex; f = fusiform cortex; m = middle temporal gyrus; s = superior temporal gyrus; e = extrastriate visual cortex; p = primary (striate) visual cortex.

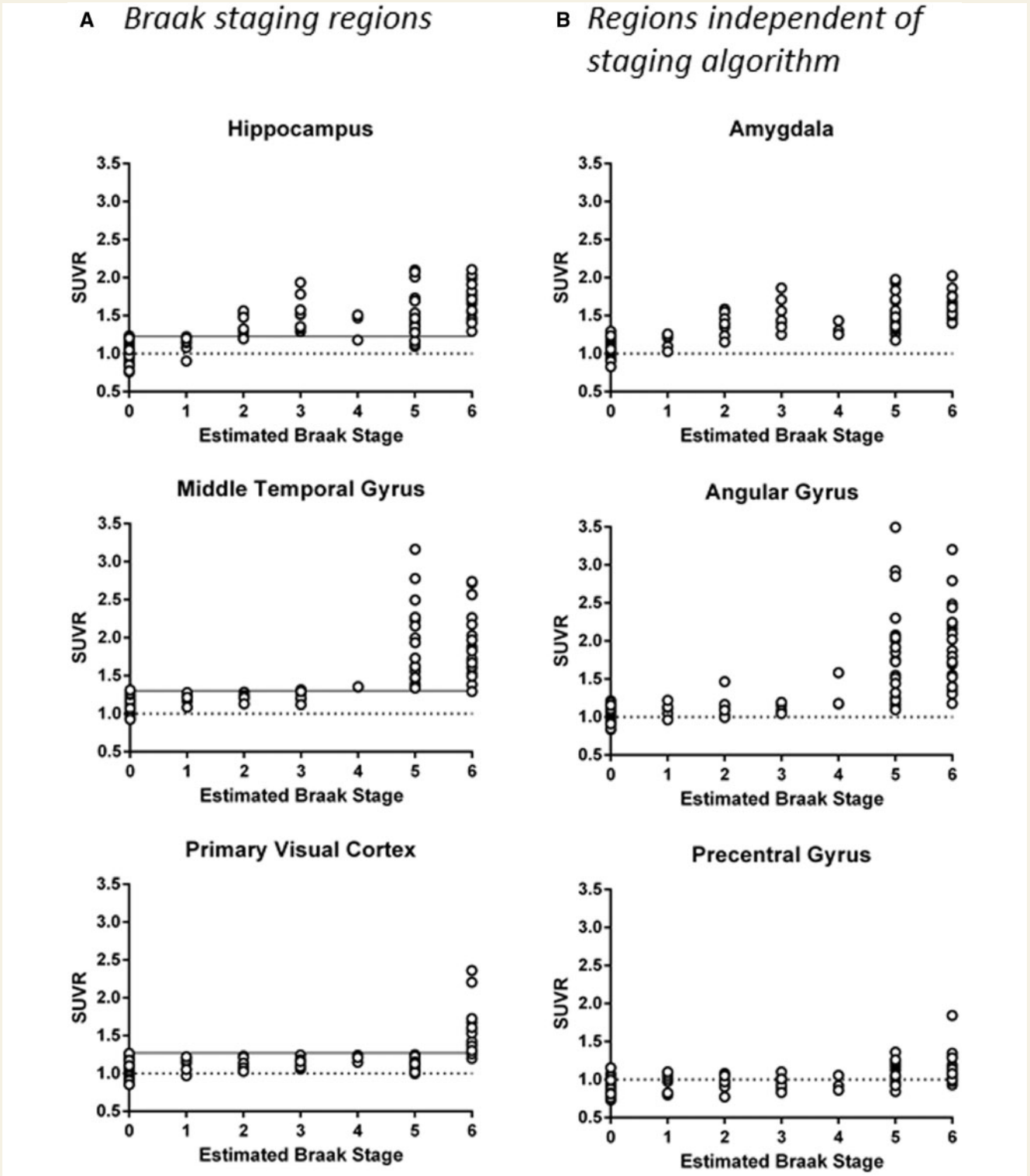

Figure 4 Image signal intensity (SUVR), averaged across left and right hemispheres, for individual subjects as a function of estimated Braak stage. Although the trend for the mean values is to increase with more advanced stage, there is substantial variability across subjects in supra-threshold signal, especially for regions in association cortices. (**A**) Three regions used in the Braak staging algorithm. (**B**) Three regions independent of the Braak staging algorithm.

that are similar to the distributions of tau pathology observed in neuropathological studies. This provides an important parallel to gold standard post-mortem results and is consistent with the *ex vivo* evidence (Xia *et al.*, 2013; Marquie *et al.*, 2015) that this tracer acts as a selective marker of tau pathology in living subjects. In particular, by sampling the images at sentinel brain regions in the anterior temporal and occipital lobes used in the neuropathological staging procedure (Braak *et al.*, 2006), an *in vivo* Braak stage was able to be estimated by a simple profile-matching mathematical algorithm. The identified profiles recapitulated expected patterns across these regions and more widespread involvement of other cortical areas in the advanced stages (Braak and Braak, 1991).

In the current sample of 173 subjects, patterns consistent with those expected from Braak stages 0 through VI were observed, including focal uptake in the transentorhinal region (consistent with Braak I/II and the earliest stages of tau spreading) and distributions increasingly involving lateral temporal lobe and occipital structures in sequences expected from Braak stages IV–VI. Evaluated against the estimated Braak stage as a measure of disease progression, SUVR values outside the specific regions used in the staging algorithm increased in a similar fashion, with limbic regions increasing first, followed by association cortices and primary sensory areas last of all. Although the vast majority of subjects exhibited an anatomical tau profile consistent with one of the predefined stereotypical or variant profiles, a small number (12/173, 7%) had suprathreshold tau signal distributions that did not conform to one the expected patterns in either hemisphere. Several of these subjects had relative sparing of parts of the medial and inferior temporal lobe despite suprathreshold signal in lateral temporal and/or occipital cortex, and one Alzheimer's disease subject exhibited strong and widespread binding but sparing of the transentorhinal cortex. These patterns may be related to the hippocampal sparing subtype of Alzheimer's disease recently proposed (Murray *et al.*, 2011). Two subjects were positive only in the hippocampus bilaterally. More relaxed decision rules, in which a Braak stage is estimated based on the region of interest furthest along the sequence of expected involvement (i.e. not requiring 'earlier' regions to be positive) would stage two of these subjects as stage II, one as stage IV, nine as stage V and one as stage VI (Supplementary material).

The Braak staging procedure—and our implementation of it for *in vivo* PET images—is a measure of spread of the pathology (to the degree it can be estimated from cross-sectional data), but does not take account of signal intensity variation above the binarization thresholds. In addition to the atypical (unclassified) patterns mentioned above, the subjects with predefined typical or variant profiles exhibited a wide range of suprathreshold image intensities and SUVR values in staging regions and other brain areas, especially those in the association cortices. This variation is not accounted for in the present staging algorithm but increased tau burden in different brain regions may provide important additional information relating to subject cognitive or functional status, and could provide an important window on heterogeneity in the disease population (Murray *et al.*, 2011). Indeed, regional SUVR values correlated more strongly with measures of global cognition than did the estimated Braak stage itself, suggesting that the density of tau pathology provides additional information beyond the degree to which it has spread beyond the mesial temporal lobes.

Our current staging approach was based closely on the proposed post-mortem procedure (Braak *et al.*, 2006), although in practice a neuropathological assessment takes account of other brain regions when they are available and, like a radiological read, may reflect a gestalt interpretation of all the information available (Braak and Braak, 1991). Given that the whole brain is invariably sampled in imaging studies, modified *in vivo* staging schemes could be developed that routinely take account of both a wider range of brain regions and the degree of signal intensity. However, intersubject variability in intensity and differential involvement of other brain areas may be better analysed outside of a staging scheme *per se*. The regions used in the present algorithm and proposed by Braak appear to reliably capture the progression (degree of spread of tau pathology) in most subjects in the current sample.

We observed a significant association between the estimated Braak stage and diagnostic category, amyloid status and measures of global cognition. These findings are consistent with tau as a major pathological driver of the disease process and with the significant relationship between tau and amyloid pathology in Alzheimer's disease that has been reported in neuropathological studies (Thal *et al.*, 2002; Braak *et al.*, 2011). One of the major current models of Alzheimer's disease invokes independent accumulation of isocortical amyloid and medial temporal tau, with amyloid triggering an accelerated spread of tau via as yet undetermined mechanisms (Jack, 2014). The present data are consistent with a link between these two pathological markers. However, we also observed a minority of divergent cases, either amyloid negative with non-zero estimated Braak stage, or amyloid positive with the Braak stage estimated to be zero. The former may represent cases of primary age-related tauopathy (PART) (Crary *et al.*, 2014), although we note that low levels of amyloid-β plaques may be present but below the level of detection of amyloid PET imaging (Clark *et al.*, 2012; Murray *et al.*, 2015; Thal *et al.*, 2015). These subjects may thus also reflect an early, pre-symptomatic Alzheimer's disease stage. Such subjects would also be interesting to evaluate further with imaging markers of neurodegeneration [structural imaging or fluorodeoxyglucose (FDG)-PET] to assess their relationship to populations with Alzheimer's disease-like clinical symptoms and neurodegeneration signatures but normal brain amyloid levels, termed suspected non-amyloid pathology (SNAP) (Jack, 2014). Four amyloid negative older control or MCI subjects were staged as Braak V–VI; visual inspection of these scans revealed a similar pattern of diffuse elevated cortical signal, slightly stronger in the anterior temporal lobes but also involving white matter in the neocortex

(Supplementary material). Moreover, as 'pure Alzheimer's disease' (abnormal amyloid and tau pathology only) appears to be a relatively rare occurrence in sporadic disease (Toledo *et al.*, 2013), co-pathologies unmeasured in the present study may also explain some of these divergent cases and variability in the presentation of tau pathology. Indeed, although the relationships were statistically significant, the predictor variables diagnosis, amyloid status and global cognition only explained ~20% of the variance in the estimated Braak stage in each model, reinforcing the point that this staging approach serves to gauge the spread of tau pathology in the brain but other factors beyond spread *per se* are likely important determinants of function.

Overall, the prevalence of the estimated non-zero Braak stages was lower than that expected based on large-scale neuropathological studies, which estimate that ~80% of 60 year olds will have neurofibrillary tangles at least in the transentorhinal cortex (Braak *et al.*, 2011). This may reflect the lower sensitivity of the ^{18}F-AV-1451 PET imaging compared with neuropathological procedures, with a substantial number of neurofibrillary tangles required to yield a reliably quantifiable PET signal. Thus, in any individual the *in vivo* estimated Braak stage could be lower than that which would be assigned post-mortem. The nature of this relationship can be refined in future autopsy studies obtaining *in vivo* PET imaging and post-mortem neuropathology in the same subjects.

We based our *in vivo* staging algorithm on the methodological protocol that was designed for uniform application in neuropathological examinations and, as a result, very clearly specified in terms of histological sections, anatomical delineation and associated decision rules (Braak *et al.*, 2006). These Braak staging criteria, instantiated as successive involvement of key brain structures, were easily translated into our algorithm based on a binarization (positive or negative by brain region) of the tau PET signal. This neuropathological protocol represents an operational evolution of the original Braak staging scheme (Braak and Braak, 1991) and encapsulated in the recent NIA-AA guidelines. Those guidelines recommend that the 7-level staging scheme is reduced to a 4-level one, with stages I–II, III–IV and V–VI, respectively, combined for improved reliability (Montine *et al.*, 2012). Our algorithm assigns seven stages 0 through VI, but adjacent categories can easily be combined for compatibility with the NIA-AA guidelines (Fig. 3). A European consortium has recommended a slight variant on the Braak staging scheme, using a semiquantitative scoring of AT8-stained tau pathology (Alafuzoff *et al.*, 2008). Brain regions assessed in this scheme comprised the anterior hippocampus at the level of the uncus, the posterior hippocampus at the level of lateral geniculate nucleus, the middle and superior temporal gyri, and the occipital cortex including the calcarine fissure, along with the inferior parietal lobule and middle frontal gyrus. Overall, the proposed staging decision rules are highly consistent with those proposed by Braak, and the parietal and frontal regions are not explicitly used in the staging instructions (Alafuzoff *et al.*, 2008) (Table 2). However, the semiquantitative scoring system is less easily translated into decision rules for ^{18}F-AV-1451 PET images, and the inter-rater agreement for this scheme was relatively poor for all but the most advanced stages.

Limitations

The present analysis used a set of small, focal regions of interest in standard brain template space to sample the 3D brain images at precise locations to correspond to the Braak histological protocol. Although a non-linear, MRI-driven, spatial transformation of the data was used to map each PET scan onto the template, and grey matter masking was used to maximize specificity of the signals, some residual mismatch between the individual and template anatomy is possible. From a neuropathological perspective, the early spread of tau pathology beyond the transentorhinal cortex in Braak stage II involves the CA1/CA2 subfields of the hippocampus specifically. However, this level of anatomical detail is difficult to resolve reliably in PET images. Our hippocampal region of interest covered the anterior most part of the hippocampus without distinction between subfields. This likely limits the extent to which Braak stages I and II can be reliably distinguished using ^{18}F-AV-1451. Equally, the choice of specific cut-point(s) for positivity was not systematically optimized, but would be an area of future investigation when larger sample sizes (enabling independent training and test sets) and, especially, when within-subject imaging and autopsy data (providing a gold standard against which an algorithm may be optimized) are available. Also, the effects of different PET cameras and reconstruction algorithms, affecting the intrinsic spatial resolution of the ^{18}F-AV-1451 images, were not evaluated in the present study and might be an important factor to consider further. Finally, as discussed above, the *in vivo* PET scanning is likely to be less sensitive than neuropathological examination (similar to the case for amyloid tracers), with a substantial number of neurofibrillary tangles required to yield a PET signal reliably quantifiable above the background.

Conclusions

The ability to image tau pathology in living humans represents a substantial advance in the study of neurodegenerative diseases, and could enable tau pathology to be measured and tracked across disease types and longitudinally as they progress. In this cross-sectional study of 173 older control, MCI and Alzheimer's disease subjects, we demonstrated the presence of anatomical profiles of increased ^{18}F-AV-1451 binding that strongly mirrored the stereotypical spread and progression of tau pathology that is encapsulated in the Braak staging scheme. A quantitative profile-matching algorithm was able to assign a predefined stereotypical or variant profile, and associate a plausible estimated Braak stage, to

most subjects. Regional tracer uptake profiles consistent with Braak stages 0 through VI were observed, although several atypical patterns were also noted. The estimated Braak stage was significantly associated with global cognition, diagnostic category and brain amyloid load. In addition to underscoring the face validity of the tracer, an *in vivo* tau staging scheme would provide a flexible yet principled means to select or group subjects in the research and assessment of neurological disease. Combined with biomarkers of amyloid-β, it provides a more complete assessment of Alzheimer's pathology in the living brain.

Funding

Data acquisition was funded by Siemens and Avid Radiopharmaceuticals, a wholly-owned subsidiary of Eli Lilly and Company. The analytical work performed in the preparation of this report was funded by Avid Radiopharmaceuticals and Eli Lilly and Company in the form of salaries paid to the authors.

Supplementary material

Supplementary material is available at *Brain* online.

References

Alafuzoff I, Arzberger T, Al-Sarraj S, Bodi I, Bogdanovic N, Braak H, et al. Staging of neurofibrillary pathology in Alzheimer's disease: a study of the BrainNet Europe Consortium. Brain Pathol 2008; 18: 484–96.

Albert MS, DeKosky ST, Dickson D, Dubois B, Feldman HH, Fox NC, et al. The diagnosis of mild cognitive impairment due to Alzheimer's disease: recommendations from the National Institute on Aging-Alzheimer's Association workgroups on diagnostic guidelines for Alzheimer's disease. Alzheimers Dement 2011; 7: 270–9.

Amunts K, Kedo O, Kindler M, Pieperhoff P, Mohlberg H, Shah NJ, et al. Cytoarchitectonic mapping of the human amygdala, hippocampal region and entorhinal cortex: intersubject variability and probability maps. Anat Embryol (Berl) 2005; 210: 343–52.

Braak H, Alafuzoff I, Arzberger T, Kretzschmar H, Del Tredici K Staging of Alzheimer disease-associated neurofibrillary pathology using paraffin sections and immunocytochemistry. Acta Neuropathol 2006; 112: 389–404.

Braak H, Braak E Neuropathological stageing of Alzheimer-related changes. Acta Neuropathol 1991; 82: 239–59.

Braak H, Thal DR, Ghebremedhin E, Del Tredici K Stages of the pathologic process in Alzheimer disease: age categories from 1 to 100 years. J Neuropathol Exp Neurol 2011; 70: 960–9.

Buchhave P, Minthon L, Zetterberg H, Wallin AK, Blennow K, Hansson O Cerebrospinal fluid levels of beta-amyloid 1-42, but not of tau, are fully changed already 5 to 10 years before the onset of Alzheimer dementia. Arch Gen Psychiatry 2012; 69: 98–106.

Chien DT, Bahri S, Szardenings AK, Walsh JC, Mu F, Su MY, et al. Early clinical PET imaging results with the novel PHF-tau radioligand [F-18]-T807. J Alzheimers Dis 2013; 34: 457–68.

Clark CM, Pontecorvo MJ, Beach TG, Bedell BJ, Coleman RE, Doraiswamy PM, et al. Cerebral PET with florbetapir compared with neuropathology at autopsy for detection of neuritic amyloid-β plaques: a prospective cohort study. Lancet Neurol 2012; 11: 669–78.

Crary JF, Trojanowski JQ, Schneider JA, Abisambra JF, Abner EL, Alafuzoff I, et al. Primary age-related tauopathy (PART): a common pathology associated with human aging. Acta Neuropathol 2014; 128: 755–66.

Hyman BT, Phelps CH, Beach TG, Bigio EH, Cairns NJ, Carrillo MC, et al. National Institute on Aging-Alzheimer's Association guidelines for the neuropathologic assessment of Alzheimer's disease. Alzheimers Dement 2012; 8: 1–13.

Jack CR Jr. PART and SNAP. Acta Neuropathol 2014; 128: 773–6.

Jack CR, Knopman DS, Jagust WJ, Petersen RC, Weiner MW, Aisen PS, et al. Tracking pathophysiological processes in Alzheimer's disease: an updated hypothetical model of dynamic biomarkers. Lancet Neurol 2013; 12: 207–16.

Joshi A, Pontecorvo M, Lu M, Skovronsky DM, Mintun M, Devous MD A semi-automated method for quantification of florbetapir F 18 PET images. J Nucl Med 2015; 56: 1736–41.

Marquie M, Normandin MD, Vanderburg CR, Costantino I, Bien EA, Rycyna LG, et al. Validating novel tau PET tracer [F-18]-AV-1451 (T807) on postmortem brain tissue. Ann Neurol 2015; 78: 787–800.

Maruyama M, Shimada H, Suhara T, Shinotoh H, Ji B, Maeda J, et al. Imaging of tau pathology in a tauopathy mouse model and in Alzheimer patients compared to normal controls. Neuron 2013; 79: 1094–108.

McKhann GM, Knopman DS, Chertkow H, Hyman BT, Jack CR Jr, Kawas CH, et al. The diagnosis of dementia due to Alzheimer's disease: recommendations from the National Institute on Aging-Alzheimer's Association workgroups on diagnostic guidelines for Alzheimer's disease. Alzheimers Dement 2011; 7: 263–9.

Montine TJ, Phelps CH, Beach TG, Bigio EH, Cairns NJ, Dickson DW, et al. National Institute on Aging-Alzheimer's Association guidelines for the neuropathologic assessment of Alzheimer's disease: a practical approach. Acta Neuropathol 2012; 123: 1–11.

Murray ME, Graff-Radford N, Ross OA, Petersen RC, Duara R, Dickson D Neuropathologically defined subtypes of Alzheimer's disease with distinct clinical characteristics: a retrospective study. Lancet Neurol 2011; 10: 785–96.

Murray ME, Lowe VJ, Graff-Radford NR, Liesinger AM, Cannon A, Przybelski SA, et al. Clinicopathologic and 11C-Pittsburgh compound B implications of Thal amyloid phase across the Alzheimer's disease spectrum. Brain 2015; 138 (Pt 5): 1370–81.

Okamura N, Harada R, Furumoto S, Arai H, Yanai K, Kudo Y Tau PET imaging in Alzheimer's disease. Curr Neurol Neurosci Rep 2014; 14: 500.

Stancu IC, Vasconcelos B, Terwel D, Dewachter I Models of beta-amyloid induced Tau-pathology: the long and "folded" road to understand the mechanism. Mol Neurodegener 2014; 9: 51.

Thal DR, Beach TG, Zanette M, Heurling K, Chakrabarty A, Ismail A, et al. [(18)F]flutemetamol amyloid positron emission tomography in preclinical and symptomatic Alzheimer's disease: specific detection of advanced phases of amyloid-beta pathology. Alzheimers Dement 2015; 11: 975–85.

Thal DR, Rub U, Orantes M, Braak H Phases of Abeta-deposition in the human brain and its relevance for the development of AD. Neurology 2002; 58: 1791–800.

Toledo JB, Cairns NJ, Da X, Chen K, Carter D, Fleisher A, et al. Clinical and multimodal biomarker correlates of ADNI neuropathological findings. Acta Neuropathol Commun 2013; 1: 65.

Toledo JB, Xie SX, Trojanowski JQ, Shaw LM Longitudinal change in CSF Tau and Abeta biomarkers for up to 48 months in ADNI. Acta Neuropathol 2013; 126: 659–70.

Villemagne VL, Okamura N In vivo tau imaging: obstacles and progress. Alzheimers Dement 2014; 10 (Suppl 3): S254–64.

Xia CF, Arteaga J, Chen G, Gangadharmath U, Gomez LF, Kasi D, et al. [(18)F]T807, a novel tau positron emission tomography imaging agent for Alzheimer's disease. Alzheimers Dement 2013; 9: 666–76.